

## Two-Step Synthesis of V<sub>2</sub>O<sub>5</sub> Nanosheets with High Sensing Properties toward Acetone

Hai-Tao FU<sup>a</sup>, Zhi-Kui ZHANG<sup>b</sup>, Xiao-Hong YANG\* and Xi-Zhong An<sup>c</sup>

School of Metallurgy, Northeastern University, Shenyang 110819, China

yangxh@smm.neu.edu.cn

**Keywords:** Vanadium pentoxide, nanosheets, hydrothermal method, gas sensing

**Abstract.** Vanadium pentoxide (V<sub>2</sub>O<sub>5</sub>) nanosheets are successfully synthesized by a hydrothermal method, followed by a high-temperature sintering treatment. Several advanced techniques are used to characterize the morphology and composition of the nanostructures, such as transmission electron microscope (TEM), high-resolution TEM (HRTEM), scanning electron microscope (SEM), and X-ray diffraction (XRD). The HRTEM image and selected area electron diffraction (SAED) indicate the crystalline grows along [010] direction. The gas sensing performance of the V<sub>2</sub>O<sub>5</sub> nanosheets was evaluated toward several volatile organic compounds (VOCs), such as ethanol, acetone, pyridine, and formaldehyde. The results show that the nanosheets exhibits superior sensing response and selectivity toward acetone to that of commercial V<sub>2</sub>O<sub>5</sub> particles at optimum working temperature of ~300°C. this work will help explore vanadium oxides as sensing materials towards VOCs with high performance.

### Introduction

Vanadium pentoxide nanoparitics, as an n-type semiconductor, has been widely studied in many fields (such as gas sensors, lithium ion battery, and catalysts) due to its unique layered structure, high chemical stability, low manufacturing cost, and high resistance to corrosion. Recently, gas sensing property of V<sub>2</sub>O<sub>5</sub> toward VOCs has been attracted increasing attention, which makes V<sub>2</sub>O<sub>5</sub> exhibit high potentials for drunken driving tests, indoor gas detection, and even disease diagnosis. [1, 2] Meanwhile, sensing performances of such materials are highly shape-dependent toward some VOCs, such as ethanol,[3] organic ammine,[4] and acetone.[5] Various morphologies such as nanowires,[4] belts,[1] rods,[2] sheets,[6] even 3D structures (urchin-like,[5] flower-like,[7] hollow spheres[8]) have been reported to detect VOCs. For instance, V<sub>2</sub>O<sub>5</sub> nanobelts (1 μm × 30 nm), prepared by a hydrothermal method, show short response/recovery times of 30-50s and a low detection limit (5 ppm) toward ethanol.[3] However, there still exists a great challenge to control nanostructure with desirable morphologies for excellent sensing performance toward volatile gases.

Acetone is a toxic, flammable gas, which is widely used as solvent, chemical intermediate, medicine and cosmetic intermediate. More importantly, acetone was found to diagnosis disease. It is found that over two hundred of VOCs are in human breath.[9] The concentration of various VOCs is the key factor for diagnosis use. Among these VOCs, acetone is proved as a biomarker for determining diabetes via human breath, but the concentration should be at sub-ppm level.[10] Currently, the techniques for detecting acetone mainly focus on table-top equipment, such as Gas Chromatography-Mass Spectrometry (GC-MS) and Proton Transfer Reaction-Mass Spectrometry (PTR-MS) which are expensive and not suitable for portable carrier. Resis-chemical sensors are proposed as a low-cost, high efficient and convenient tool to detect acetone.[10] However, sensing materials are vital to the sensing performance.

For detecting acetone, various metal oxide nanoparticles have been investigated for detection of acetone. For instance, ZnO thin film can be used to detect acetone at 200°C with sensitivity of 5.71.[11] TiO<sub>2</sub> thin film was reported to detect acetone at 500°C with sensitivity of 4.[12] Furthermore, various morphologies of WO<sub>3</sub> nanoparticles show good sensitivity toward acetone.[10] Despite of the efforts above, the sensing performance of these materials toward acetone are unsatisfactory for practical use, and still requires further enhancement.

Herein, we report a two-step method for synthesis of  $V_2O_5$  nanosheets for sensing acetone. The morphology and composition of such structures will be characterized with several analytical techniques, such as transmission electron microscopy (TEM), high-resolution transmission electron microscopy (HRTEM), scanning electron microscopy (SEM), X-ray diffraction (XRD). The gas sensing performance (e.g., sensitivity, selectivity, and stability) of the as-prepared  $V_2O_5$  nanoparticles toward several VOCs (including acetone) will be measured and evaluated.

## Experimental Method

### Synthesis of $V_2O_5$ Nanosheets

In a typical synthesis procedure, commercialized  $V_2O_5$  (0.14g) were added in 16 ml of ethylene glycol (EG) with vigorous stirring at 60 °C for several hours until the color of the suspension changed from brownish yellow to light yellow. Then, a certain amount of HCl (23%) was used to adjust the pH (~1) of the system. 20 ml of such obtained suspension was added into a 50 ml Teflon container. After the container was sealed in an autoclave, it was heated at 260°C for 24 hours. After cooled down to room temperature naturally, the resulting black precipitate was collected by centrifugation, washed thoroughly with deionized water and ethanol several times and finally dried at 70°C overnight before further use. Finally, the precipitate was sintered at 400°C in the atmosphere of air for 2 hours, respectively.

### Characterization

The phase composition and purity of the synthesized particles were examined using Phillips X'pert Multipurpose X-ray Diffraction System (MPD) equipped with graphite mono-chromatized  $Cu-K\alpha$  radiation ( $\lambda=1.54 \text{ \AA}$ ) in the  $2\theta$  range of 10-80°. The particle morphologies were observed on a JEOL 1400 microscope (TEM), operated at an accelerated voltage of 100 kV. HRTEM images were recorded on a JEM 2100F field emission transmission electron microscope with an accelerating voltage of 200 kV. SEM images were recorded with a JEM-7001F field emission scanning electron microscope.

### Gas Sensor Construction and Measurements

The gas sensors were fabricated according to the procedures reported in our previous studies.[13, 5] Specifically, the as-prepared  $V_2O_5$  particles were first dispersed in ethanol to form slurry, which was then coated on a ceramic tube with previously printed Au electrodes and Pt conducting wires. The ceramic tube was subsequently dried at 100 °C for 2 h to evaporate the solvent. To be stable, all the materials were treated and aged at 300 °C in air until the resistance became stable (~24h). The sensing properties of the  $V_2O_5$  particles were evaluated using a computer-controlled WS-30A gas-sensing measurement system (Weisheng Electronics Co., Ltd., Henan, China).

Before the measurement, a Ni-Cr resistor was inserted into the ceramic tube as a heater, which is used to control the operating temperature by adjusting the heating voltage ( $V_{\text{heating}}$ ). A reference resistor was placed in series with the sensor to form a complete measurement circuit. The change of the voltage at the two ends of the reference resistor ( $R_{\text{reference}}$ ) can be monitored by the computer. The target gas (e.g., 1-butylamine) was injected into the testing chamber using a microsyringe. The response (S) of n-type semiconductors can be defined as the ratio of the resistances measured in air ( $R_a$ ) and in the tested gas atmosphere ( $R_g$ ):  $S=R_a/R_g$ . The output voltage was set at 5 V and the gas-sensing measurements were conducted at a relative humidity of 55-65%.

## Results and Discussion

### Composition of the as-Prepared Precursors and Final Products

The phase composition of vanadium oxide precursors and  $V_2O_5$  nanosheets was characterized by XRD, as shown in Fig. 1a. The figure depicts the XRD patterns of the precursors (curve a) and  $V_2O_5$

nanosheets (curve b). It can be seen that  $V_2O_3$ , labeled as diamond, is the domain compound in the precursors. Other peaks can be indexed as vanadyl ethylene glycolate (VEG) ( $2\theta=13.6^\circ$ , labeled as circle), VOOH ( $2\theta=27.2^\circ$ , labeled as square) and some unknown species ( $2\theta=47.8^\circ$  and  $76.9^\circ$ , labeled as triangle). Curve b shows the typical XRD patterns of the pure  $V_2O_5$ , corresponding to the sintered products of the precursors. All of the diffraction peaks can be well indexed to the diffraction peaks of orthogonal phase of  $V_2O_5$  (JCPDS 01-089-0612). Due to the  $V_2O_5$  product sintered from the precursors, it can be deduced that the unknown species in the precursor are still vanadium species.

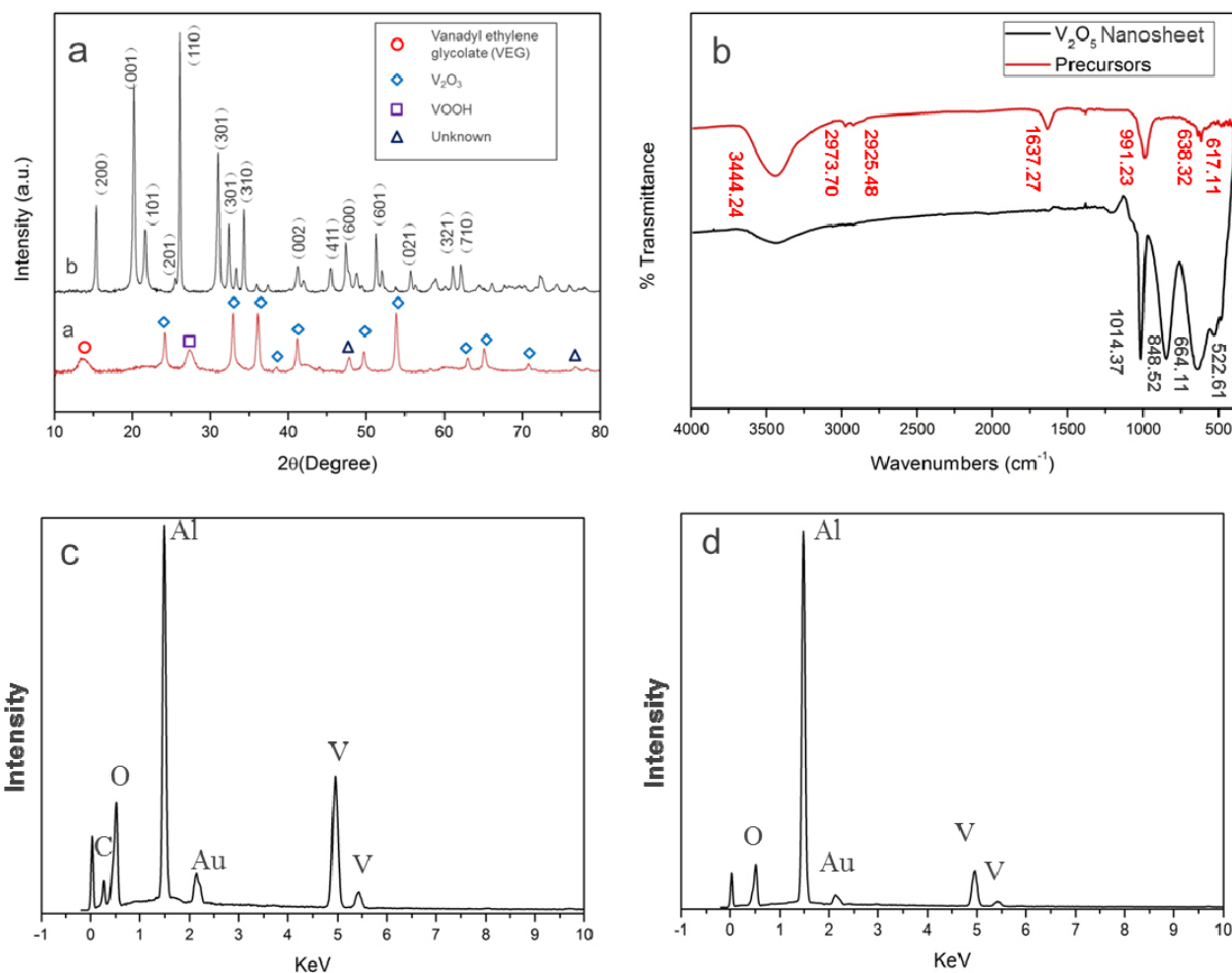


Fig. 1 (a) XRD patterns of precursors (curve a) and  $V_2O_5$  nanosheets (curve b). (b) FT-IR patterns of the precursor and  $V_2O_5$  nanosheets. EDS patterns of the precursor (c) and the as-prepared  $V_2O_5$  (d).

To further confirm the composition of the precursor and investigate the transformation from precursor to  $V_2O_5$ , FT-IR was used to characterize the functional group of the precursor and final product, as shown in Fig.1b. It can be clearly seen that there are two strong broad peaks located at  $\sim 3444$  and  $1637\text{ cm}^{-1}$  for precursor curve, while these peaks are not obvious in final product curve. This indicates that O-H bond exists in precursors, which may generate from VOOH species. The small peaks located at  $\sim 2973$  and  $2925\text{ cm}^{-1}$  represent  $CH_2O$ - group, probably originated from VEG. The peak centered at  $\sim 991\text{ cm}^{-1}$  can be assigned to  $V=O$  stretching bond, while those centered at  $638$  and  $617\text{ cm}^{-1}$  are attributed to the  $V-O-V$  bending mode and coupled bending vibration of  $V-O$ . From the FT-IR spectra, it can be confirmed that the VEG and VOOH species exist in the precursor, in good agreement with the deduction from the XRD pattern. The black curves in Fig. 1b shows a typical FT-IR spectrum of  $V_2O_5$ , in which the  $V=O$  stretching bond appears at  $\sim 1014\text{ cm}^{-1}$ . While the peak at  $522\text{ cm}^{-1}$  is assigned to the  $V-O-V$  stretching bond. The  $V-O$  stretching bond and the coupled vibration between  $V=O$  and  $V-O-V$  bonds can be found at  $664$  and  $848\text{ cm}^{-1}$ , respectively.[5, 14] Fig. 1c and d show the elemental EDS spectra of the precursor and sintered  $V_2O_5$  products, respectively. The EDS

spectrum of precursor clearly indicates the existence of carbon, due to the presence of VEG; while the peak corresponding to carbon (C) vanishes in the EDS spectrum of  $V_2O_5$ . The element of aluminium (Al) is generated from sample holders, while Au is attributed to Au spin-coating for SEM observation.

### Morphology of the as-Prepared Precursors and the Final Products

The morphology of the products was inspected by microscopic techniques. Fig.2a shows the SEM image of the nanosheets, indicating that the nanosheets are with thickness of  $\sim 10$  nm. Fig.2b displays the TEM image of the nanosheets, and the high resolution TEM (HRTEM) and selected diffraction pattern (SAED) of the circle is exhibited in Fig.2c and d, respectively. The HRTEM reveals that the lattice fringes were clearly visible with a lattice spacing of 0.44 nm, which can be assigned to (001) planes of  $V_2O_5$ , with growth direction along [010]. The SAED pattern shows two typical orthorhombic crystalline planes are indexed as (101) and (200), which is in good agreement with HRTEM image.[15]

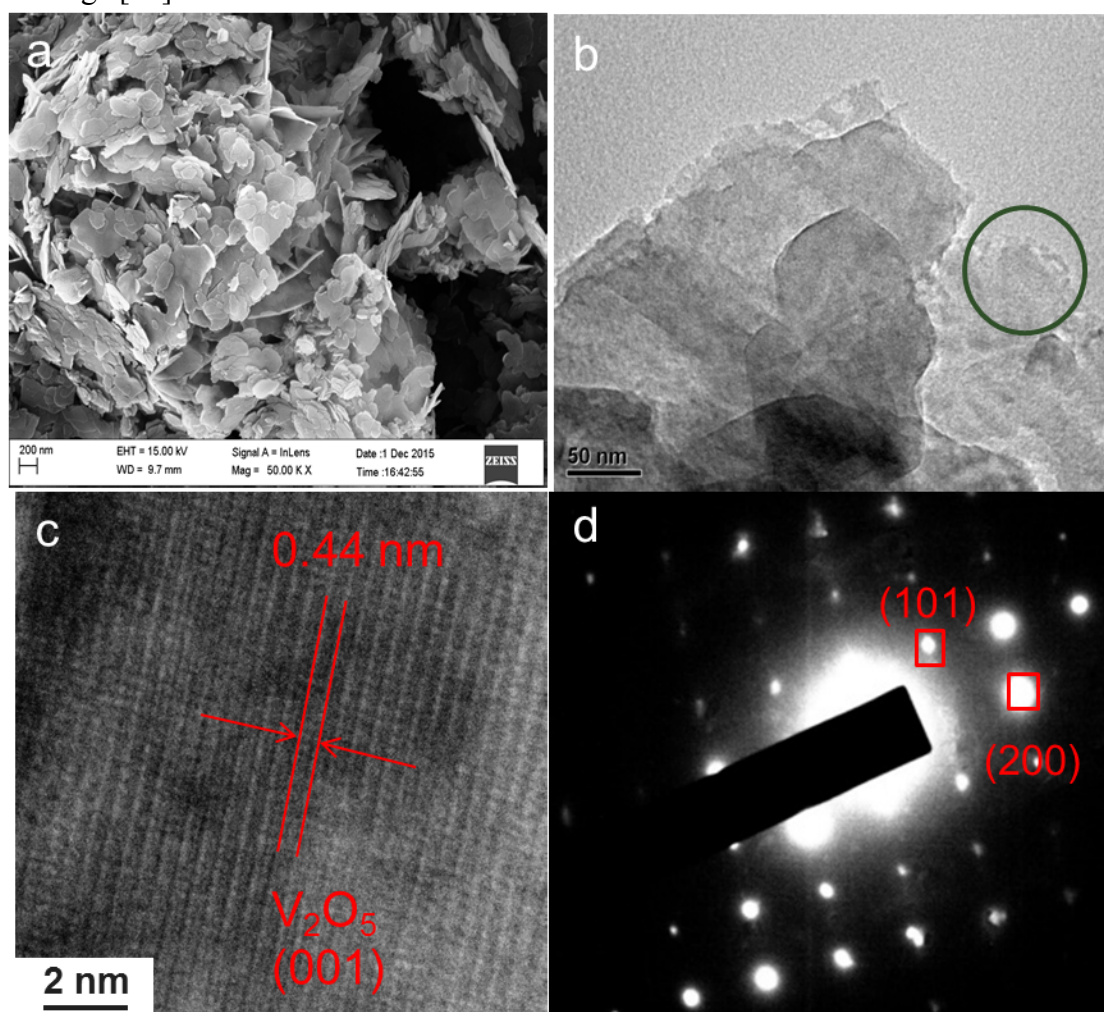


Fig. 2 (a) SEM image of the  $V_2O_5$  nanosheets; (b) TEM image of the nanosheets; (c) the HRTEM image of the nanosheets at the circular area in Fig.2b; (d) the corresponding SAED pattern of Fig.2c.

### Gas Sensing Performance

The gas sensing performance of the  $V_2O_5$  nanosheets was investigated via measuring the selectivity to ethanol, acetone, pyridine, isopropanol and formaldehyde. In comparison, the commercial  $V_2O_5$  particles were used as sensing material. As an n-type semiconductor,  $V_2O_5$  is expected to adsorb O and OH groups which trap electrons from the conduction band of the  $V_2O_5$  crystals and increase the resistance. The adsorbed oxygen and lattice oxygen of  $V_2O_5$  can react with gas molecules which are chemical adsorbed at the active sites on the surface of  $V_2O_5$  materials. In this process, electrons will transfer to the surface of  $V_2O_5$  to lower the number of trapped electrons, which induces a decrease in the resistance.[16]



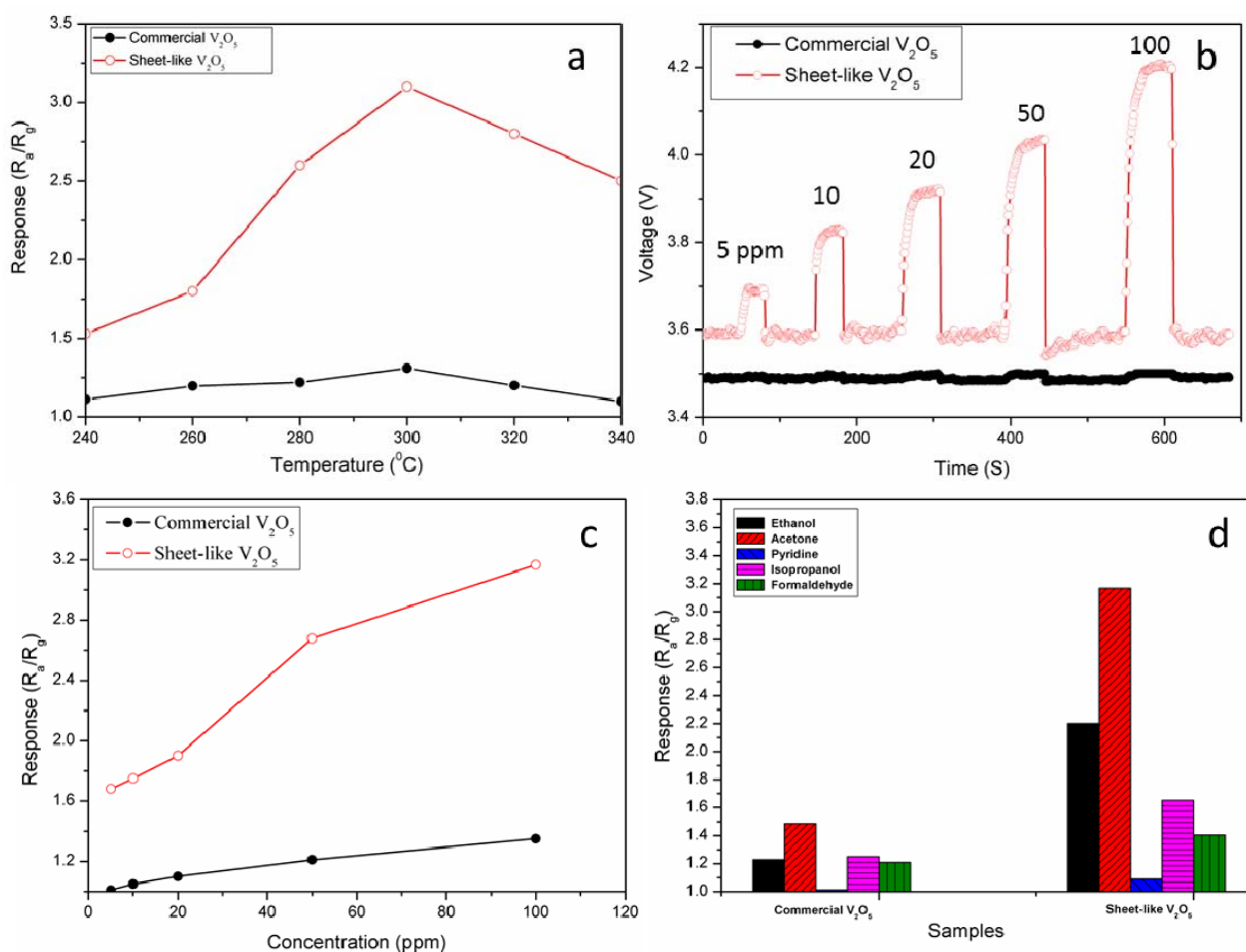


Fig. 3 (a) Response to 100 ppm acetone of the sensors based on the sheet-like V<sub>2</sub>O<sub>5</sub> particles, and commercial V<sub>2</sub>O<sub>5</sub> particles at various working temperatures. (b) Sensor voltage transient curve of the sheet-like and commercial V<sub>2</sub>O<sub>5</sub> particles to various concentration of acetone at the optimum working temperature of 300°C. (c) Response of the three V<sub>2</sub>O<sub>5</sub> particles to different concentration of acetone testing at the optimum temperature. (d) Relative selectivity of the sensors based on the two V<sub>2</sub>O<sub>5</sub> particles to various gases at the optimum working temperature, while the gas concentration is fixed at 100 ppm.

The diffusion rates of gas molecules are dependent on temperatures, thus the working temperature significantly may affect both the response and the sensitivity. Fig. 3a displays the response of the sensors made from the V<sub>2</sub>O<sub>5</sub> nanosheets and the commercial V<sub>2</sub>O<sub>5</sub> particles toward 100 ppm of acetone with increasing working temperature from 240–340°C. All V<sub>2</sub>O<sub>5</sub> microflower-based sensors exhibit an optimum working temperature of 300°C with  $S=3.1$  toward 100 ppm of acetone. In comparison, the commercial V<sub>2</sub>O<sub>5</sub> based sensors show the same optimum working temperatures, but the responses are lower than that of V<sub>2</sub>O<sub>5</sub> nanosheets.

The dynamic response-recovery transients of the V<sub>2</sub>O<sub>5</sub>-based sensors are shown in Fig. 3b. It is obvious that the output voltages of the sensors increase when the acetone is input, and decrease with the removal of the gas. Fig. 3c depicts the responses of three V<sub>2</sub>O<sub>5</sub> based sensors toward different concentrations of acetone at 300°C. It can be seen that the V<sub>2</sub>O<sub>5</sub> nanosheets show much higher response (~3 times) towards acetone than the commercial V<sub>2</sub>O<sub>5</sub> particles.

Selectivity is another critical characteristic in gas sensing, which needs to be evaluated to ensure an accurate detection of a single gas in a mixer with a higher response. The response of the sensors based on the flower-like the sheet-like and the commercial V<sub>2</sub>O<sub>5</sub> particles towards 100 ppm of different gases (e.g., acetone, pyridine, formaldehyde and alcohols) were measured at the working temperature of 300 °C, as displayed in Fig. 3d. It is noted that the sheet-like V<sub>2</sub>O<sub>5</sub> exhibit excellent selectivity to acetone, with much higher response than that of other gases. In comparison, the high selectivity

towards acetone is observed on the sensors based on the sheet-like  $V_2O_5$  particles, while the selectivity of the commercial  $V_2O_5$  particles is not ideal. This indicates that the morphology of the  $V_2O_5$  particles could highly affect the selectivity.

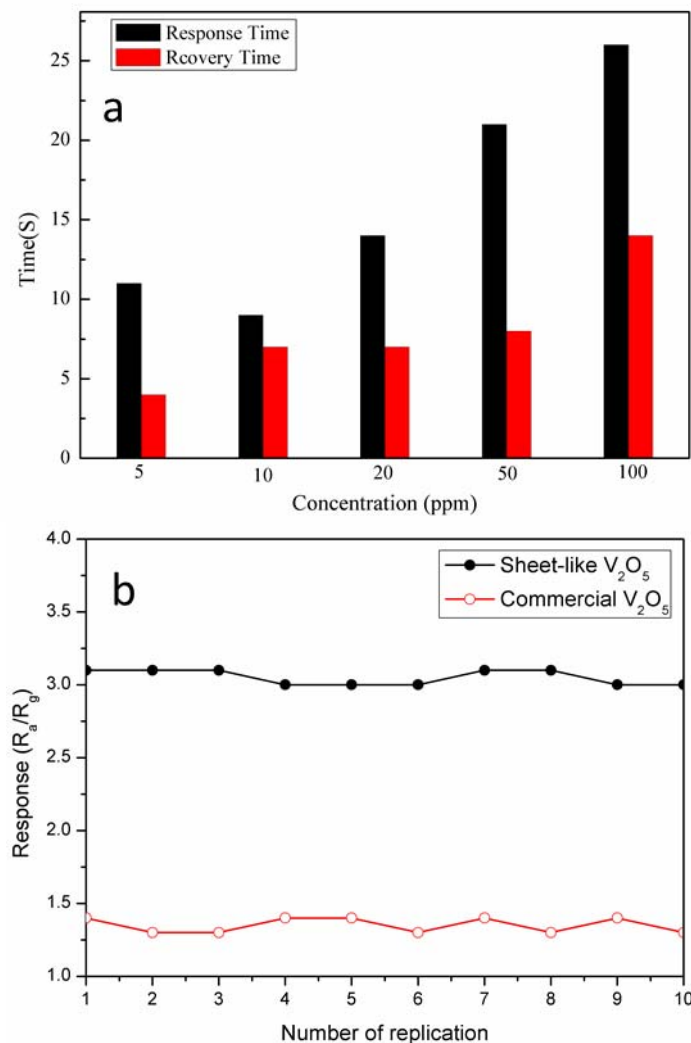


Fig. 4 (a) Response and recovery time values of the sheet-like  $V_2O_5$  particles; (b) Repeatability tests of the two samples toward 100 ppm of acetone for repeating 10 times at 300°C.

Recover time is also a key criterion to judge gas sensing performance of nanoparticles. Fig. 4a shows the response/recovery time of the sheet-like  $V_2O_5$  particles. The response time is defined as the time required to 90% of the final equilibrium value, following exposure to acetone vapor. Inversely, the recovery time is defined as the time needed by the sensor to return to 10% of the original conductance in air, with removal of acetone vapor. It can be observed that the response time of the sheet-like  $V_2O_5$  particles (Fig. 4a) upon exposure to 5-100 ppm of acetone differs from 10-25 s, whereas the recovery time is 3-14 s. Additionally, we also observed that the response/recovery time increases with gas concentration, probably due to the low vapor and diffusion rate of acetone in the gas chamber at high concentration. The above results show that the response speed of the sheet-like  $V_2O_5$  particles is slower than that of commercial  $V_2O_5$  particles. It can be concluded that the nanosheet can enhance the sensitivity and selectivity to acetone of  $V_2O_5$  particles, however, the response speed slightly decreased.

Repeatability is one of important parameters of a sensing material, related to long-term reliability of the sensor. As shown in Fig. 4b, the repeatabilities of the samples (the sheet-like, and commercial  $V_2O_5$  particles) were evaluated by testing the response towards 100 ppm of acetone at 300 °C by repeating 10 times. It can be found that the response of the sensing materials remains constant during 10 tests,

suggesting the excellent potential of the sheet-like  $V_2O_5$  as a sensitive, selective and stable sensing material for detection of acetone.

## Conclusions

A facile and synthesis strategy by combination of hydrothermal method and sintering treatment to prepare  $V_2O_5$  nanosheets has been demonstrated. Sheet-like  $V_2O_5$  nanopaticles have been obtained under the reported conditions with thickness of  $\sim 10$  nm. Furthermore, the sheet-like  $V_2O_5$  nanoparticles show excellent gas sensing performance toward acetone. The nanosheets show a low detection limit to 5 ppm and a significant high selectivity toward acetone at the optimum working temperature of  $300^\circ\text{C}$ . The sheet-like particles show short response (11-25 s) and recovery time (4-13 s) at the concentration range from 5-100 ppm under the reported conditions. The results in this work provide the potential use of vanadium oxide nanoparticles for industrial and environmental applications in the future.

## Acknowledgment

We gratefully acknowledge the financial support of the National Natural Science Foundation of China (No. 51404066), the National Basic Research Program of China (N150204011), and the China Postdoctoral Science Foundation (No. 2015M581353).

## References

- [1] C.L. Niu, J.B. Li, H.B. Jin, H.L. Shi, Y.Q. Zhu, W.Z. Wang, M.S. Cao. Self-template processed hierarchical  $V_2O_5$  nanobelts as cathode for high performance lithium ion battery. *Electrochimica Acta*. 182 (2015) 621-8.
- [2] J. Chu, Z.Z. Kong, D.Y. Lu, W.L. Zhang, X.S. Wang, Y.F. Yu, S. Li, X.Q. Wang, S.X. Xiong, J. Ma. Hydrothermal synthesis of vanadium oxide nanorods and their electrochromic performance. *Materials Letters*. 166 (2016) 179-82.
- [3] J.F. Liu, X. Wang, Q. Peng, Y.D. Li. Vanadium pentoxide nanobelts: Highly selective and stable ethanol sensor materials. *Adv Mater*. 17 (2005) 764.
- [4] I. Raible, M. Burghard, U. Schlecht, A. Yasuda, T. Vossmeier.  $V_2O_5$  nanofibres: novel gas sensors with extremely high sensitivity and selectivity to amines. *Sensor Actuat B-Chem*. 106 (2005) 730-5.
- [5] H. Fu, X. Jiang, X. Yang, A. Yu, D. Su, G. Wang. Glycothermal synthesis of assembled vanadium oxide nanostructures for gas sensing. *Journal of Nanoparticle Research*. 14 (2012) 1-14.
- [6] H.Q. Song, C.P. Zhang, Y.G. Liu, C.F. Liu, X.H. Nan, G.Z. Cao. Facile synthesis of mesoporous  $V_2O_5$  nanosheets with superior rate capability and excellent cycling stability for lithium ion batteries. *Journal of Power Sources*. 294 (2015) 1-7.
- [7] Y. Qin, G. Fan, K. Liu, M. Hu. Vanadium pentoxide hierarchical structure networks for high performance ethanol gas sensor with dual working temperature characteristic. *Sensors and Actuators B: Chemical*. 190 (2014) 141-8.
- [8] J. Pan, L. Zhong, M. Li, Y.Y. Luo, G.H. Li. Microwave-Assisted Solvothermal Synthesis of  $VO_2$  Hollow Spheres and Their Conversion into  $V_2O_5$  Hollow Spheres with Improved Lithium Storage Capability. *Chemistry-a European Journal*. 22 (2016) 1461-6.
- [9] A. Manolis. The diagnostic potential of breath analysis. *Clinical chemistry*. 29 (1983) 5-15.

- [10] S.-J. Choi, I. Lee, B.-H. Jang, D.-Y. Youn, W.-H. Ryu, C.O. Park, I.-D. Kim. Selective Diagnosis of Diabetes Using Pt-Functionalized WO<sub>3</sub> Hemitube Networks As a Sensing Layer of Acetone in Exhaled Breath. *Analytical Chemistry*. 85 (2013) 1792-6.
- [11] N. Kakati, S.H. Jee, S.H. Kim, J.Y. Oh, Y.S. Yoon. Thickness dependency of sol-gel derived ZnO thin films on gas sensing behaviors. *Thin Solid Films*. 519 (2010) 494-8.
- [12] A. Teleki, S.E. Pratsinis, K. Kalyanasundaram, P.I. Gouma. Sensing of organic vapors by flame-made TiO<sub>2</sub> nanoparticles. *Sensors and Actuators B: Chemical*. 119 (2006) 683-90.
- [13] H. Fu, H. Xie, X. Yang, X. An, X. Jiang, A. Yu. Hydrothermal Synthesis of Silver Vanadium Oxide (Ag<sub>0.35</sub>V<sub>2</sub>O<sub>5</sub>) Nanobelts for Sensing Amines. *Nanoscale Research Letters*. 10 (2015) 411.
- [14] E.M. Guerra, G.R. Silva, M. Mulato. Extended gate field effect transistor using V<sub>2</sub>O<sub>5</sub> xerogel sensing membrane by sol-gel method. *Solid State Sci*. 11 (2009) 456-60.
- [15] H. Yu, X. Rui, H. Tan, J. Chen, X. Huang, C. Xu, W. Liu, D.Y.W. Yu, H.H. Hng, H.E. Hoster, Q. Yan. Cu doped V<sub>2</sub>O<sub>5</sub> flowers as cathode material for high-performance lithium ion batteries. *Nanoscale*. 5 (2013) 4937-43.
- [16] B. Sun, J. Horvat, H.S. Kim, W.-S. Kim, J. Ahn, G. Wang. Synthesis of Mesoporous  $\alpha$ -Fe<sub>2</sub>O<sub>3</sub> Nanostructures for Highly Sensitive Gas Sensors and High Capacity Anode Materials in Lithium Ion Batteries. *The Journal of Physical Chemistry C*. 114 (2010) 18753-61.